

The effect of realistic equations of state and general relativity on the “snowplow” model for pulsar glitches.

S. Seveso^{1,2}, P. M. Pizzochero,^{1,2*} B. Haskell³

¹*Dipartimento di Fisica, Università degli Studi di Milano, Via Celoria 16, 20133 Milano, Italy*

²*Istituto Nazionale di Fisica Nucleare, sezione di Milano, Via Celoria 16, 20133 Milano, Italy*

³*Astronomical Institute “Anton Pannekoek”, University of Amsterdam, Postbus 94249, 1090 GE Amsterdam, the Netherlands*

11 October 2021

ABSTRACT

Many pulsars are observed to “glitch”, i.e. show sudden jumps in their rotational frequency ν , some of which can be as large as $\Delta\nu/\nu \approx 10^{-6} - 10^{-5}$ in a subset of pulsars known as giant glitchers. Recently Pizzochero (2011) has shown that an analytic model based on realistic values for the pinning forces in the crust and for the angular momentum transfer in the star can describe the average properties of giant glitches, such as the inter-glitch waiting time, the step in frequency and that in frequency derivative. In this paper we extend the model (originally developed in Newtonian gravity and for a polytropic equation of state) to realistic backgrounds obtained by integrating the relativistic equations of stellar structure and using physically motivated equations of state to describe matter in the neutron star. We find that this more detailed treatment still reproduces the main features of giant glitches in the Vela pulsar and allows us to set constraints on the equation of state. In particular we find that stiffer equations of state are favoured and that it is unlikely that the Vela pulsar has a high mass (larger than $M \approx 1.5M_{\odot}$).

Key words: stars:neutron - pulsars:general - pulsars:individual:PSR B0833-45

1 INTRODUCTION

Many pulsars are observed to “glitch”, i.e. they show sudden increases in their spin frequency that are instantaneous to the accuracy of the data. To date several hundreds of glitches have been detected (Espinoza et al. 2011), with relative increases in the spin frequency ν that range from as low as $\Delta\nu/\nu \approx 10^{-11}$ to $\Delta\nu/\nu \approx 10^{-5}$. In particular a class of pulsars, of which the Vela pulsar is the prototype, exhibit what are known as “giant” glitches (Espinoza et al. 2011), large steps in the spin frequency ($\Delta\nu/\nu \approx 10^{-6}$) which are accompanied by an increase in the spindown rate $\dot{\nu}$ and exhibit a rough periodicity in their recurrence rate (for example giant glitches in the Vela occur roughly every three years).

Shortly after the first glitches were observed it was suggested that they could be due to a superfluid component in the stellar interior, weakly coupled to the normal component and to the electromagnetic emission, that could store angular momentum and then release it catastrophically, giving rise to a glitch (Baym, Pathick & Pines 1969; Anderson & Itoh 1975; Alpar 1977; Alpar et al. 1984a). Large scale superfluid components are, in fact, expected in Neutron Star

(NS) interiors on theoretical grounds given that the temperature of the star will drop below the superfluid critical temperature (typically $\approx 10^9$ K) soon after birth. Furthermore recent observations of the cooling of the young NS in the supernova remnant Cassiopeia A have provided the first direct indication of superfluidity in NS interiors (Page et al. 2011; Shternin et al. 2011).

A superfluid rotates by forming an array of quantised vortices which carry the circulation of the fluid. In the NS crust the vortices can be strongly attracted, “pinned”, to the nuclear lattice (Anderson & Itoh 1975; Alpar 1977; Pines et al. 1980; Anderson et al. 1982) and cannot move outward. If the superfluid cannot remove vortices it cannot spin down and it therefore acts as an angular momentum reservoir. As the crust spins down due to electromagnetic emission a lag will develop between the superfluid and the normal component, leading to a hydrodynamical lift force (Magnus force) acting on the vortices. Eventually when the lag reaches a critical value the pinning force will no longer be able to contrast the hydrodynamical lift and the vortices will unpin, transferring their angular momentum to the crust and giving rise to a glitch.

Although there is some evidence that smaller glitches in young active pulsars such as the Crab may be related to

* E-mail: pierre.pizzochero@mi.infn.it

crust quakes (Crawford & Demianski 2003; Middleditch et al. 2006), there is a growing consensus that the basic picture outlined above can be used to describe the main features of pulsar glitches. There is still considerable debate on the “trigger” for vortex unpinning and several mechanisms have been proposed (including crust quakes (Ruderman 1976; Ruderman, Zhu & Chen 1998), heat release (Larson & Link 2002) and hydrodynamical instabilities (Glampedakis & Andersson 2009)), but recent work by Warszawski & Melatos (2008) (see also Melatos & Warszawski (2009); Warszawski & Melatos (2011)) has been very successful in using cellular automaton simulations that can track the movement of a large number of vortices, to reproduce the distribution of glitch sizes and waiting times, and Haskell, Pizzochero & Sidery (2012) have produced the first hydrodynamical simulation that can follow all stages of a giant glitch, from the rise to the relaxation.

One of the main difficulties in performing such calculations, up to now, has been the relative scarcity of realistic estimates of the pinning force between vortices and nuclei in the crust. However the recent calculation of Grill & Pizzochero (2012a) (see also Grill (2011); Grill & Pizzochero (2012b)) has filled this gap and produced physically consistent pinning profiles that can be used to study pulsar glitches. In fact Pizzochero (2011) has shown that these forces can be incorporated into a simple analytical model, the so-called “snowplow” model, that predicts the size, step in frequency derivative and waiting time of Vela glitches. The same forces were used by Haskell, Pizzochero & Sidery (2012) in a hydrodynamical model to reproduce also the post-glitch relaxation of Vela glitches and show that the model is consistent with the size and waiting times of other pulsars that exhibit giant glitches.

We shall discuss the details of the snowplow model in the following sections, the main assumption, however, is that vortices close to the rotational axis of the star will only be weakly pinned at their extremities. The Magnus force can thus easily unpin them and move them towards the equator, where they will repin as they are now immersed in the strong pinning region of the inner crust. This creates a vortex sheet that moves close to the maximum of the pinning potential as the star spins down. Once the maximum critical lag is reached the pinning force can no longer balance the Magnus force, and all the vorticity that has been accumulated is free to go, giving rise to a giant glitch. This also gives rise to a natural periodicity for giant glitches, although crust quakes or vortex avalanches can unpin part of the vorticity and give rise to smaller glitches before the maximum.

In this picture we implicitly assume that vortices that cross the core of the star are immersed in a low drag environment, i.e. that there is no pinning in the core and vortices are free to move out. This would not be the case if the protons in the interior are in a type II superconducting state and there is a strong interaction between magnetic flux tubes and rotational vortices (Ruderman, Zhu & Chen 1998; Link 2003). Note, however, that a large portion of the star may be in a type I superconducting state (Jones 2006) in which the magnetic field is not organised in flux tubes, but rather in macroscopic regions of normal matter, and the interactions may be much weaker (Sedrakian 2005) (although see Jones (2006) for a discussion of strong interactions in type I superconductors). Furthermore recent calculations suggest

that even if the superconductivity is of type II, the interaction between vortices and flux tubes will be weak in the presence of strong entrainment or superfluid Σ^- hyperons (Babaev 2009). In this paper we thus take the view that pinning in the core will be weak, although strong pinning of vortices to flux tubes is an intriguing possibility and will be the focus of a future publication (Haskell, Pizzochero & Seveso, in preparation).

Pizzochero (2011) and Haskell, Pizzochero & Sidery (2012) developed the model for an $n = 1$ polytrope in Newtonian gravity, in order to obtain simple analytical estimates for the glitch size. In this paper we investigate the effect on the snowplow model of Pizzochero (2011) of using realistic Equations of State (EoSs) and relativistic equations for the stellar structure. We will see that in general the model is consistent with observations and that less massive NSs (in the region of $1.2M_\odot - 1.5M_\odot$) are favoured to describe the Vela pulsar. The inclusion of realistic backgrounds and equations of state in the hydrodynamical models will be the focus of future work.

2 STELLAR STRUCTURE

As outlined above the model proposed by Pizzochero (2011) relies on calculating the amount of vorticity that can be stored in the inner crust before the Magnus force overcomes the maximum pinning force and then calculating the amount of angular momentum exchanged between the superfluid component and the crust. In order to obtain realistic estimates of the moment of inertia of the different components and of the strength of the density-dependent pinning force per unit length, it is thus important to use a realistic equation of state (EoS) for dense matter that describes the relation $P(\rho)$ between density and pressure. The stellar structure and density profile can then be obtained by integration of the Tolman-Oppenheimer-Volkov (TOV) equations:

$$\frac{dm(r)}{dr} = 4\pi r^2 \rho(r) \quad (1)$$

$$\frac{d\phi(r)}{dr} = \left(\frac{Gm(r)}{r^2} + 4\pi Gr \frac{P(r)}{c^2} \right) \left(1 - \frac{2Gm(r)}{c^2 r} \right)^{-1} \quad (2)$$

$$\frac{dP(r)}{dr} = - \left(\rho(r) + \frac{P(r)}{c^2} \right) \frac{d\phi}{dr}, \quad (3)$$

where $m(r)$ is the mass contained in a sphere of radius r , $\rho(r)$ is the density profile and $P(r)$ is the pressure. These differential equations model the hydrostatic equilibrium inside the star with relativistic approach and, of course, require the $P(\rho(r))$ function. The last two equations can be combined in one that gives an expression for the mass and pressure derivatives and the system can be solved with valid initial conditions. We obtain the functions that describe the star with the fourth-order Runge-Kutta method, starting at $r = 0$ with $m(0) = 0$ and $\rho(0) = \rho_c$, for a valid choice of the central density ρ_c . The integration stops when we reach the condition $\rho(R) = 10^{-8} \rho_c$ and we take R as the radius of the star. Of course the mass of the star is $M = m(R)$. As a result of this integration we have $m(r)$, $\rho(r)$ and $P(r)$ of the star as showed in Fig. 1.

We use two different EoSs:

- (i) SLy (Douchin & Haensel 2001) is a moderate EoS,

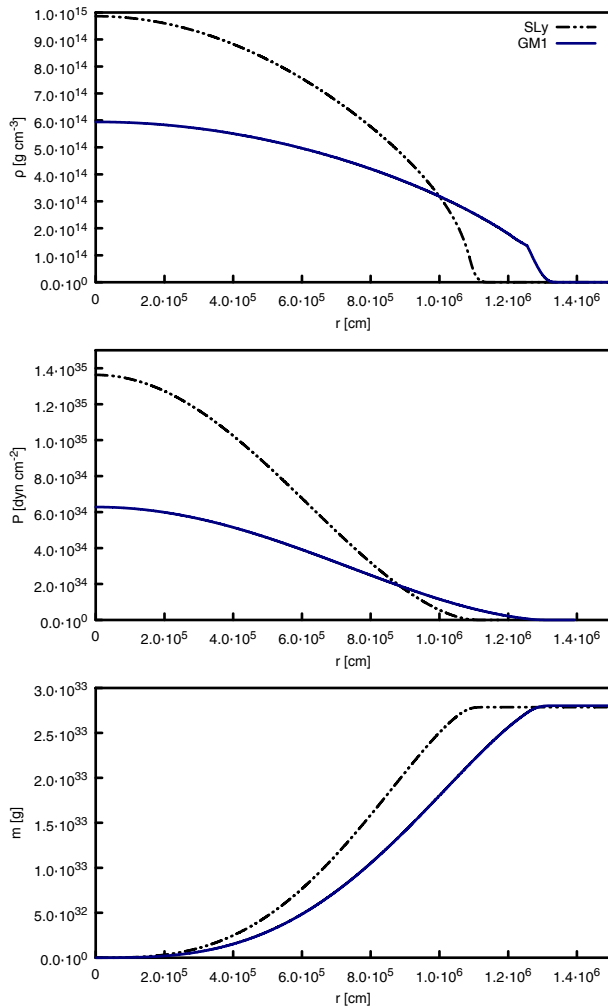


Figure 1. Mass, pressure and density profiles of $1.4 M_{\odot}$ neutron star for the EoSs considered: with fixed mass, a stiffer EoS produce a star with larger radius and lower central density.

based on a non-relativistic parametrisation; this equation describes the whole star with a single analytical expression and so it is more convenient to integrate;

(ii) GM1 by Glendenning & Moszkowski (1991) is a stiff $P(\rho)$ relation that is very similar to SLy in the crust of star, but not in the core due to different microscopic approach used to describe hadrons at densities higher than ρ_0 .

Fig. 2 shows the different mass–central density relations for the two equations of state.

This figure clearly identifies also the presence of a limit for the mass for a neutron star. The existence of a maximum mass M_{\max} is an effect of the relativistic nature of the TOV equations, where pressure contributes to the gravitational field. Of course M_{\max} depends on the EoS: a stiffer equation of state gives a higher M_{\max} . The evidence of the existence of a $2M_{\odot}$ neutron star (Demorest et al. 2010) allows, in fact, to reject soft equations of state that predict a maximum mass below this value. Table 1 shows the different values of M_{\max} for the equations of state considered.

In this work we consider stars with masses from $1M_{\odot}$ to M_{\max} . With the density profile $\rho(r)$ it is possible to identify, for each star, the structural regions that are relevant

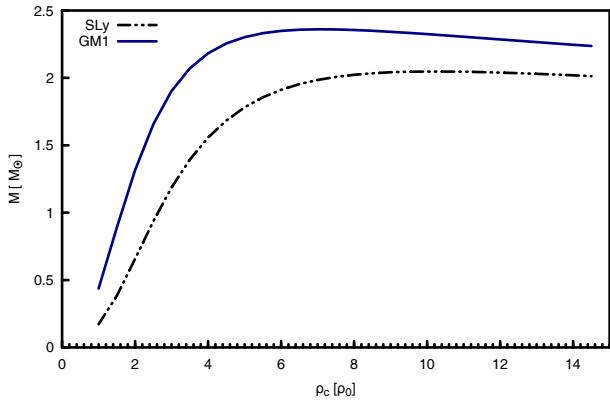


Figure 2. This plot shows the mass–central density relation for the EoSs considered. As expected, we find a maximum mass value above $2M_{\odot}$ for each equation of state (see table 1).

Table 1. This table shows, for each EoS, the maximum allowed mass with the corresponding central density ρ_c (in units of nuclear saturation density ρ_0), radius of the star R , radius of the core R_c and radius of the inner crust R_{ic} .

EoS	ρ_c (ρ_0)	M (M_{\odot})	R (km)	R_c (km)	R_{ic} (km)
SLy	10.2	2.05	9.98	9.68	9.86
GM1	7.1	2.36	11.98	11.57	11.82

for the model and important for the pinning. In particular we calculate the radius of the core R_c as the distance from the center of the star where $\rho_{\text{core}} = \rho(R_c) = 0.5\rho_0$ ($\rho_0 = 2.8 \times 10^{14} \text{ g cm}^{-3}$ is the nuclear saturation density); the inner crust–outer crust interface R_{ic} corresponds, on the other hand, to the density value $\rho_d = 0.0015\rho_0$ that is the neutron drip point: this means that in the outer crust there are no free neutrons. It is easy to calculate the moment of inertia of a shell delimited by radii r_1 and r_2 :

$$I(r_1, r_2) = \frac{8\pi}{3} \int_{r_1}^{r_2} r^4 \rho(r) dr. \quad (4)$$

We can then calculate also the moment of inertia of every region, considering that $I_{\text{core}} = I(0, R_c)$, $I_{ic} = I(R_c, R_{ic})$ and $I_{oc} = I(R_{ic}, R)$.

Table 2 shows all the relevant parameters for the considered stars, obtained from the integration of the TOV equations with SLy and GM1.

3 PINNING AND VORTICITY

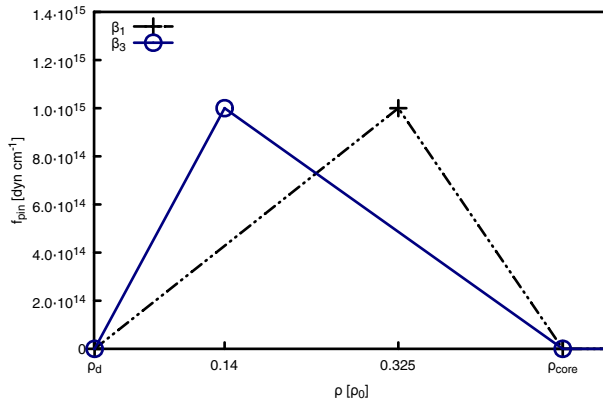
One of the most important ingredients of the model is clearly $f_{\text{pin}}(\rho)$, the pinning force per unit length that acts on the vortex line as a result of its interaction with the lattice (in the inner crust). Although the pinning force per pinning site can readily be evaluated from the knowledge of the pinning energy (Alpar 1977; Epstein & Baym 1988; Donati & Pizzochero 2003, 2004, 2006), the force per unit length of a vortex, which is the quantity that must be equated to the Magnus force in order to understand whether a vortex is

Table 2. We give all the structural parameters (as defined in section 2) of the stars used to test the snowplow model, for both EoSs tested. See also figure 3 for a graphical representation of these quantities.

EoS	M (M_{\odot})	R (km)	R_c (km)	R_{ic} (km)	I_{tot} (10^{45} g cm 2)	I_{core} (10^{45} g cm 2)	I_{ic} (10^{43} g cm 2)	I_{oc} (10^{40} g cm 2)
SLy	1.0	11.86	10.35	11.23	0.739	0.697	4.181	6.638
	1.1	11.83	10.49	11.28	0.827	0.788	3.923	5.945
	1.2	11.80	10.60	11.31	0.914	0.878	3.652	5.317
	1.3	11.76	10.69	11.32	0.999	0.965	3.370	4.738
	1.4	11.71	10.75	11.32	1.079	1.048	3.078	4.198
	1.5	11.64	10.79	11.29	1.154	1.126	2.777	3.685
	1.6	11.55	10.79	11.24	1.222	1.197	2.469	3.194
	1.7	11.42	10.76	11.16	1.279	1.258	2.150	2.718
	1.8	11.26	10.68	11.03	1.322	1.303	1.818	2.248
	1.9	11.03	10.54	10.83	1.339	1.324	1.463	1.769
2.0	10.62	10.23	10.47	1.299	1.289	1.042	1.233	
GM1	1.0	13.94	11.79	13.02	1.021	0.896	12.505	19.061
	1.1	13.94	12.01	13.12	1.146	1.025	12.068	17.532
	1.2	13.94	12.19	13.20	1.271	1.156	11.555	16.108
	1.3	13.93	12.35	13.27	1.395	1.285	10.991	14.780
	1.4	13.91	12.47	13.32	1.516	1.412	10.382	13.530
	1.5	13.89	12.58	13.34	1.634	1.536	9.738	12.340
	1.6	13.85	12.66	13.35	1.747	1.657	9.062	11.198
	1.7	13.79	12.71	13.35	1.854	1.771	8.362	10.099
	1.8	13.72	12.74	13.32	1.954	1.878	7.635	9.031
	1.9	13.62	12.74	13.26	2.043	1.974	6.885	7.987
	2.0	13.49	12.70	13.17	2.118	2.057	6.107	6.956
	2.1	13.33	12.63	13.05	2.173	2.120	5.292	5.922
	2.2	13.10	12.48	12.85	2.194	2.150	4.411	4.851
2.3	12.71	12.20	12.51	2.146	2.113	3.371	3.631	

pinned or free, is much more complex to evaluate, as it depends on the rigidity of a vortex and on its orientation with respect to the crustal lattice.

Grill & Pizzochero (2012a) (see also Grill (2011); Grill & Pizzochero (2012b)) have performed numerical simulations to evaluate this quantity, taking into account different orientation of the bcc lattice. They found that the order of magnitude of the maximum pinning force f_{PM} is approximately 10^{15} dyn cm $^{-1}$ and that there is no significant difference for the pinning force per unit length in considering vortex–nucleus interaction attractive or repulsive in different regions. Another interesting result found by Grill & Pizzochero (2012a) regards the position of the maximum f_{PM} . In this paper the authors use a density–dependent pairing gap $\Delta(\rho)$ obtained with a realistic microscopic nucleon–nucleon interaction. It is known that the polarization effects of the neutron medium reduce the pairing gap, but there is yet no agreement on how strong this suppression will be, although it seems reasonable to divide the $\Delta(\rho)$ by a factor β between 2 and 3. Grill & Pizzochero (2012a) consider the case $\beta = 1$ and $\beta = 3$ and find that for the two corresponding profiles $f_{pin}(\rho)$ the maximum is shifted at different densities, even if the parameter β is, of course, only a scaling factor on the same pairing gap profile. The precise height of the maximum thus depends on the vortex tension used in the model (although the order of magnitude remains 10^{15} dyn cm $^{-1}$) and does not affect the location of the maximum (once β is fixed). In this work we therefore constrain the exact value of the maximum amplitude of the pinning force by fitting the average waiting time between giant glitches in the Vela pulsar, as will be explained in the

**Figure 4.** The profile of the pinning force $f_{pin}(\rho)$ for the two cases $\beta = 1$ and $\beta = 3$, with a choice for the maximum of $f_{PM} = 10^{15}$ dyn cm $^{-1}$.

next sections. In figure 4 we show the two pinning profiles $f_{pin}(\rho)$ used in this work for $\beta = 1$ and $\beta = 3$ (plotted here with the choice of $f_{PM} = 10^{15}$ dyn cm $^{-1}$). The case β_1 has a maximum at $\rho \approx 0.325\rho_0$, while in the β_3 case the maximum is at $\rho \approx 0.14\rho_0$. In both configurations we take the pinning force to vanish at ρ_{core} and ρ_d , due to the fact that the lattice exists only in the crust and that in the outer crust there are no free neutrons to produce vortices.

A single vortex line will be described parallel to the rotational axis and distant from this axis by a distance x , that represent the cylindrical radius. We consider also the

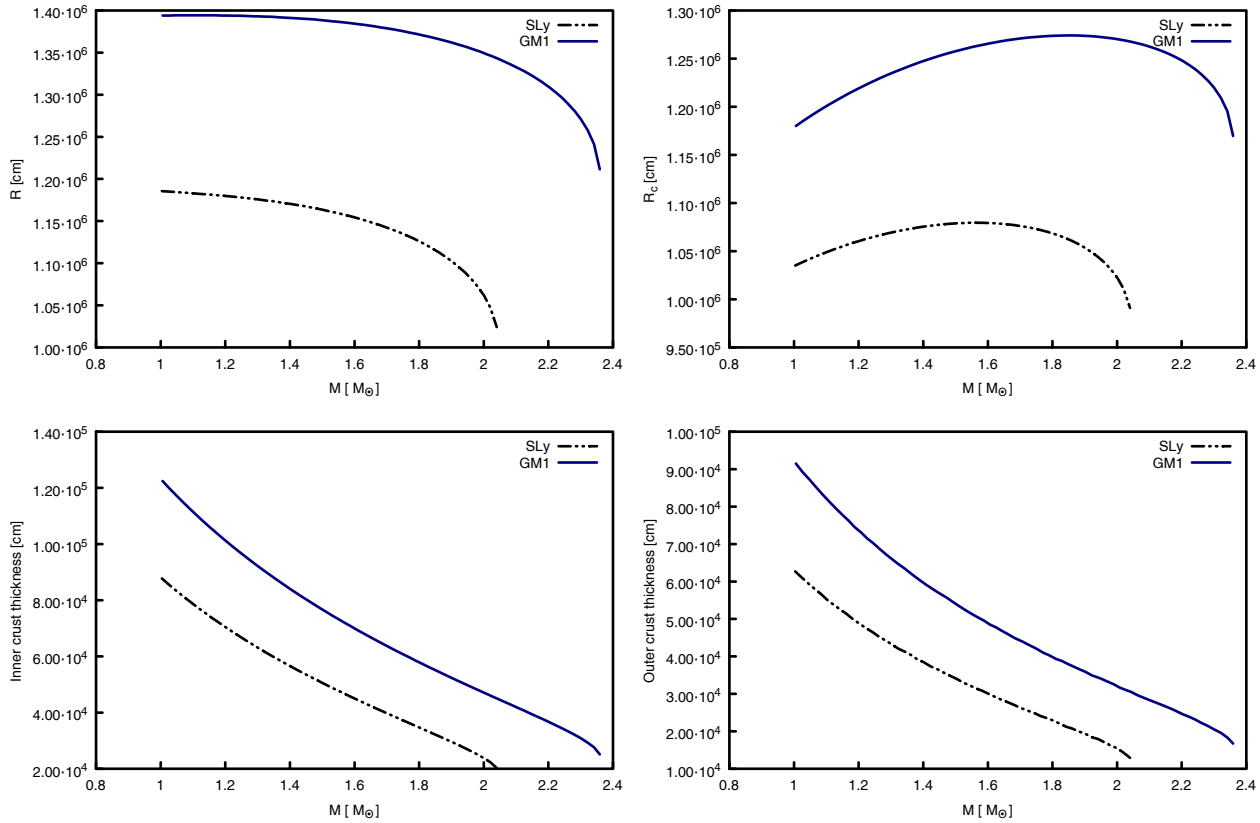


Figure 3. The first figure shows the dependence of the radius of the neutron star on the total mass, for the SLy and GM1 EoSs. The other plots represent the thicknesses of the stellar regions (core, inner crust and outer crust) as function of mass. As one can see a more massive star has thinner crusts, while a stiffer equation of state produces a larger star.

vortex line to be continuous throughout the core: there is, in fact, no theoretical evidence for the existence of an interface of normal matter between the core and the inner crust, that can justify the hypothesis of a core with vorticity separated from the crust (Zhou et al. 2004). Naturally the vortices may not be straight and parallel to the rotational axis, as turbulence may develop in the stellar interior, especially in the presence of strong pinning (Link 2011b,a). We will not consider this possibility here, but will discuss some of its likely consequences in the following.

With the above hypothesis, we can identify two (cylindrical) pinning regions based on the strength of the pinning interaction. The *strong* pinning region is defined by $x > R_c$ and corresponds to the part of the star in which the vortices lie entirely in the inner crust region, and are therefore subject to pinning for their whole length. On the other hand, in the *weak* pinning region ($x < R_c$), a vortex line is pinned only at its extremities that are immersed in the crust, while there is no pinning interaction in the core (see figure 5).

4 THE MODEL

Thanks to the axial symmetry of the problem, we can describe the macroscopic quantities of the rotating superfluid in terms of the variable $n(x)$ that represents the number of vortices per unit area, at a distance x from the rotational axis of the star. The angular velocity $\Omega_s(x)$ of the super-

fluid component of the star is in fact proportional to the number $N(x)$ of vortices enclosed in a cylindrical region of cylindrical radius x , and can be expressed as:

$$\Omega_s(x) = \frac{\kappa}{2\pi} \frac{N(x)}{x^2} = \frac{\kappa}{2\pi x^2} \int_x^{\ell(x)} n(x') da' \quad (5)$$

where the integration is performed on the area enclosed by the radius x . This result follows from the quantization of the circulation per vortex line that is encoded in the constant $\kappa = \pi\hbar/m_N$.

Once a star has been fixed by the choice of an EoS and the integration of the TOV equations, the model requires, as a first step, the evaluation of the pinning force for the whole length of a generic vortex line. This can be obtained starting from the function $f_{\text{pin}}(\rho)$ discussed previously. Let us imagine a vortex line parallel to the rotational axis of the star and distant x : the total pinning acting on it is given by the integration of $f_{\text{pin}}(\rho)$ over its length:

$$F_{\text{pin}}(x) = 2 \int_0^{\ell(x)/2} f_{\text{pin}} \left[\rho \left(\sqrt{x^2 + z^2} \right) \right] dz \quad (6)$$

where $\ell(x) = 2\sqrt{R_{\text{ic}}^2 - x^2}$ is the length of the vortex line, obtained considering that the vortex line ends at the inner–outer crust surface. To understand better the role of the pinning force, we choose a neutron star of $1.4M_\odot$ with SLy equation of state and we plot the function $F_{\text{pin}}(x)$ for x

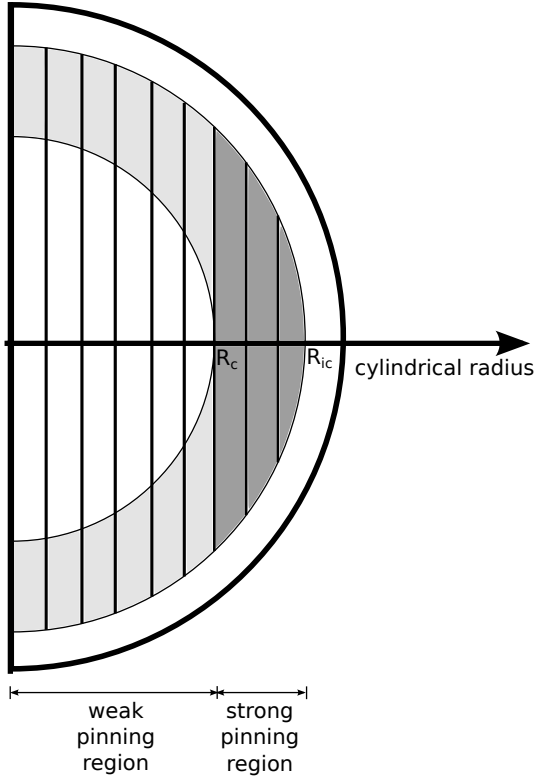


Figure 5. A schematic representation of the geometry of our problem (out of scale). The whole shaded area represents the inner crust of the NS, where vortices are pinned to the lattice. The darker part indicates the strong pinning region, where the vortices are subjected to pinning for their whole length. The star is threaded by straight continuous vortices.

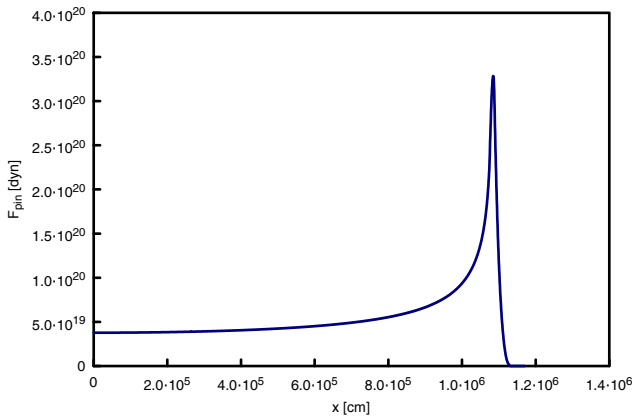


Figure 6. The total pinning force $F_{\text{pin}}(x)$ integrated on the whole length of a vortex line distant x from the rotational axis of the star. This plot is obtained taking a star of $1.4M_{\odot}$ and SLy EoS. The pinning profile used is the $\beta = 1$ case plotted in figure 4.

from 0 to R_{ic} (fig. 6, corresponding to $\beta = 1$ and $f_{\text{PM}} = 10^{15} \text{ dyn cm}^{-1}$).

The pinning interaction is not the only force that acts on a vortex line. As shown in Ruderman & Sutherland (1974), pinning prevents the vortex line from moving with the local superfluid velocity because the vortex line is compelled to have the velocity of the normal matter component (the nor-

mal component rotates as a rigid body with angular velocity Ω_c). This fact give rise to a Magnus force:

$$\mathbf{f}_m = \kappa \rho_s \mathbf{e}_z \times (\mathbf{v}_v - \mathbf{v}_s) \quad (7)$$

where \mathbf{v}_v is the velocity of the vortex line and \mathbf{v}_s is the superfluid velocity; here \mathbf{f}_m must be intended as force per unit length.

In this expression ρ_s is the density of the superfluid fraction of the star. In fact the whole star can be divided in two components: the normal one (which includes also the protons in the core as they are coupled with the crust by the magnetic field) and the superfluid one, on which the Magnus force will act. It thus follows that $\rho_s = (1 - x_p)\rho$ where x_p is the proton fraction at a given density. Of course this quantity is a microphysical property of matter and for this reason is strictly dependent on the EoS used. As this information is not provided with the EoSs used, we use the results of Zuo et al. (2004) who give the proton fraction $x_p(\rho)$ as a function of the total density in the case of two-body interactions and also in the case of three-body forces. We use both the $x_p(\rho)$ relations of Zuo et al. (2004) but we consider also a third case where the proton fraction is a constant that does not depend on the total density. We also introduce the parameter Q that represent the superfluid fraction of the star. It is defined for the general case as

$$Q = I_s / I_{\text{tot}} = \frac{\int_0^R r^4 (1 - x_p(\rho)) \rho(r) dr}{\int_0^R r^4 \rho(r) dr} \quad (8)$$

where we have used eq. 4; I_{tot} is the total moment of inertia and I_s is the moment of inertia of the superfluid component. In the case of a constant proton fraction it then follows that $Q = 1 - x_p$. The average value is $Q \approx 0.95$ and therefore we shall test our model also with this prescription.

The Magnus force in 7 has only one component in the radial direction (\mathbf{v}_v and \mathbf{v}_s are, in fact, directed along \mathbf{e}_θ , so the cross product is directed along \mathbf{e}_x) and therefore can be rewritten as:

$$\mathbf{f}_m(x, z) = f_m(x, z) \mathbf{e}_x = -\kappa \rho_s(x, z) x \Delta \Omega(x) \mathbf{e}_x \quad (9)$$

where the difference of the two velocities is written as $\Delta v(x) = x \Delta \Omega(x) = x [\Omega_c - \Omega_s(x)]$ and depends only on the coordinate x , as described by equation 5. This quantity is negative between two glitches because the normal component spins slower than the superfluid one; indeed the Magnus force is a hydrodynamical lift that pushes the vortex outward from the rotational axis. The key point here is the fact that the normal component spins down as a consequence of the loss of energy by electromagnetic radiation of the star: the result is an increase of $f_m(x, z)$ in the time interval between glitches.

The same integration performed with f_{pin} over the length of the vortex can be done with the Magnus force. We can consider the total Magnus force acting on a vortex line distant x from the rotational axis:

$$\begin{aligned} F_m(x) &= 2 \int_0^{\ell(x)/2} f_m(x, z) dz \\ &= 2 \kappa x \Delta \Omega(x) \int_0^{\ell(x)/2} \rho_s \left(\sqrt{x^2 + z^2} \right) dz. \end{aligned} \quad (10)$$

The basic idea here is to compare the pinning force and the Magnus force to find the critical lag $\Delta \Omega_{\text{cr}}(x)$ that repre-

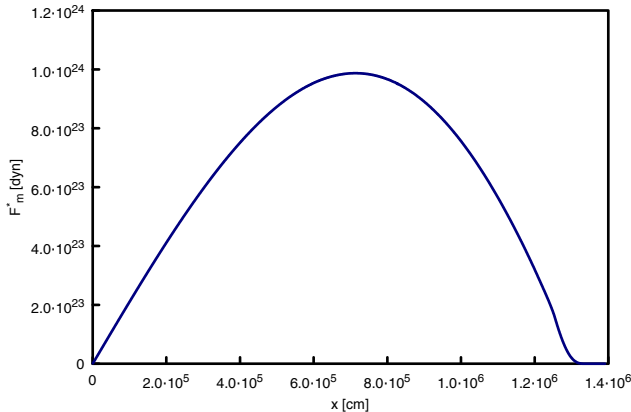


Figure 7. Plot of the expression $F_m^*(x) = F_m(x)/\Delta\Omega(x)$ as a function of the cylindrical radius x . This plot is obtained taking a star of $1.4M_\odot$ and SLy EoS.

sents the depinning condition: when the actual lag between the two components of the stars reaches the value $\Delta\Omega_{\text{cr}}$ at some point with cylindrical radius x , the vortices here are unbound from the lattice, as the Magnus force now exceeds the pinning interaction that held the vortices in place:

$$F_{\text{pin}}(x) = F_m(x) = \Delta\Omega_{\text{cr}}(x)F_m^*(x) \quad (11)$$

Here $F_m^*(x) = F_m(x)/\Delta\Omega_{\text{cr}}(x)$ and it is plotted in fig. 7 using the same reference star as in fig. 6. The important quantity is therefore the critical lag that can be easily evaluated as:

$$\Delta\Omega_{\text{cr}}(x) = \frac{\int_0^{\ell(x)/2} f_{\text{pin}}[\rho(\sqrt{x^2+z^2})] dz}{\kappa x \int_0^{\ell(x)/2} \rho_s(\sqrt{x^2+z^2}) dz}. \quad (12)$$

In figure 8 we plot the critical lag for sample stars from table 2.

It is important to point out that the critical lag shows a peak $\Delta\Omega_{\text{cr,max}} = \Delta\Omega_{\text{cr}}(x_{\text{max}})$ in a region that corresponds to the inner crust, that is the region where the pinning is stronger. In this region our estimate of $\Delta\Omega_{\text{cr}}(x)$ is reasonable since pinning is continuous along the whole single vortex. This is not the case for the critical lag in the core, because here pinning acts on vortices only at their extremities: as explained by Pizzochero (2011) this fact is responsible of the *weak* pinning in this region, even though we can assume that the system maintains axial symmetry due to the collective rigidity of vortex bundles (Ruderman & Sutherland 1974).

As the star slows down, the depinning condition $\Delta\Omega(x) \geq \Delta\Omega_{\text{cr}}(x)$ is first reached in the *core*: as shown by Link (2009), in this region repinning is dynamically possible if the lag falls below a critical value (smaller than the one for depinning). This suggest the following interpretation: in the *core*, as the star slows down, the vortices are continuously depinned and repinned, establishing a dynamical creep that removes the excess vorticity on short timescales. Furthermore the Magnus force in the interior is likely to overcome the tension of vortices and depin them long before the unpinning condition in the crust is met (Adams, Cieplak & Glaberson 1984; Haskell, Pizzochero & Sidery 2012). The conclusion is thus that vortices in the core can essentially be considered free. In this region the scattering of electrons off magnetised vortex cores is mainly responsible for the drag

forces and for the short relaxation timescale $\tau_c \sim 1 - 10$ s (Alpar et al. 1984b; Andersson, Sidery & Comer 2006): this means that we can consider the normal and the superfluid components in the core as coupled with a lag of order $|\dot{\Omega}|\tau_c$.

In the time between glitches, the depinning region becomes larger, involving also the crust: in the inner crust the excess vorticity is repinned and creates a thin vortex sheet that moves toward the peak: this sheet is pushed outward by the increasing Magnus force and it stores angular momentum. When the peak is reached, there is no more pinning interaction that can block the excess vorticity: this vorticity is suddenly released and reaches the outer crust. At this moment the angular momentum stored by vortices is transferred to the normal component of the star, and this causes the glitch.

It is straightforward now to evaluate the time interval between two glitches: this is given by the time needed to create a lag $\Delta\Omega_{\text{cr,max}}$

$$\Delta t_{\text{gl}} = \frac{\Delta\Omega_{\text{cr,max}}}{|\dot{\Omega}|} \quad (13)$$

where $\dot{\Omega}$ is the deceleration of the normal component referred to the pre-glitch steady-state condition.

The above arguments indicates that, immediately before a glitch, a lag of $\Delta\Omega_{\text{cr,max}}$ will have been created for $x = x_{\text{max}}$. This means that we can use equation 5 to express the number of vortices stored at the peak in the sheet just before a glitch:

$$N_v = \frac{2\pi}{\kappa} x_{\text{max}}^2 \Delta\Omega_{\text{cr,max}}. \quad (14)$$

Due to the particular shape of the critical lag in figure 8, we can assume that in this moment the excess vorticity in the region $x > x_{\text{max}}$ has been entirely removed by the Magnus force, and therefore the N_v vortices are the only ones responsible for the transfer of angular momentum to the normal component of the star. To evaluate the angular momentum transfer we start from the definition $dL = \Omega_s(x) dI_s$. As we are interested in the angular momentum stored by N_v vortices at the peak of the pinning potential, we use the relation in 14 and perform the integration on the cylindrical region $x_{\text{max}} < x < R_c$ to obtain the requested quantity (the integration on the coordinate x stops at R_c due to the fact that in the outer crust there is no superfluid component):

$$\Delta L_{\text{gl}} = 2\kappa N_v \int_{x_{\text{max}}}^{R_c} x dx \int_0^{\ell(x)} \rho_s(\sqrt{x^2+z^2}) dz. \quad (15)$$

Following the arguments above, at the moment of a glitch only a fraction of the core superfluidity is coupled to the normal component of the star: in fact, the rise time of a glitch (τ_{gl}) is very short and only the instantaneously depinned fraction of vorticity in the core can respond to the variation of the angular velocity of the crust. We introduce the parameter Y_{gl} to encode this fractional quantity. In fact the best observational upper limit is of $\tau_{\text{gl}} < 40$ s for the Vela 2000 glitch (Dodson, McCulloch & Lewis 2002), while an interesting lower limit of $\tau_{\text{gl}} > 10^{-4}$ ms can be set by the non-detection of gravitational waves from the Vela 2006 glitch (Warszawski & Melatos 2012). Theoretical estimates suggest that $\tau_{\text{gl}} \approx 1 - 10$ s (Haskell, Pizzochero & Sidery 2012).

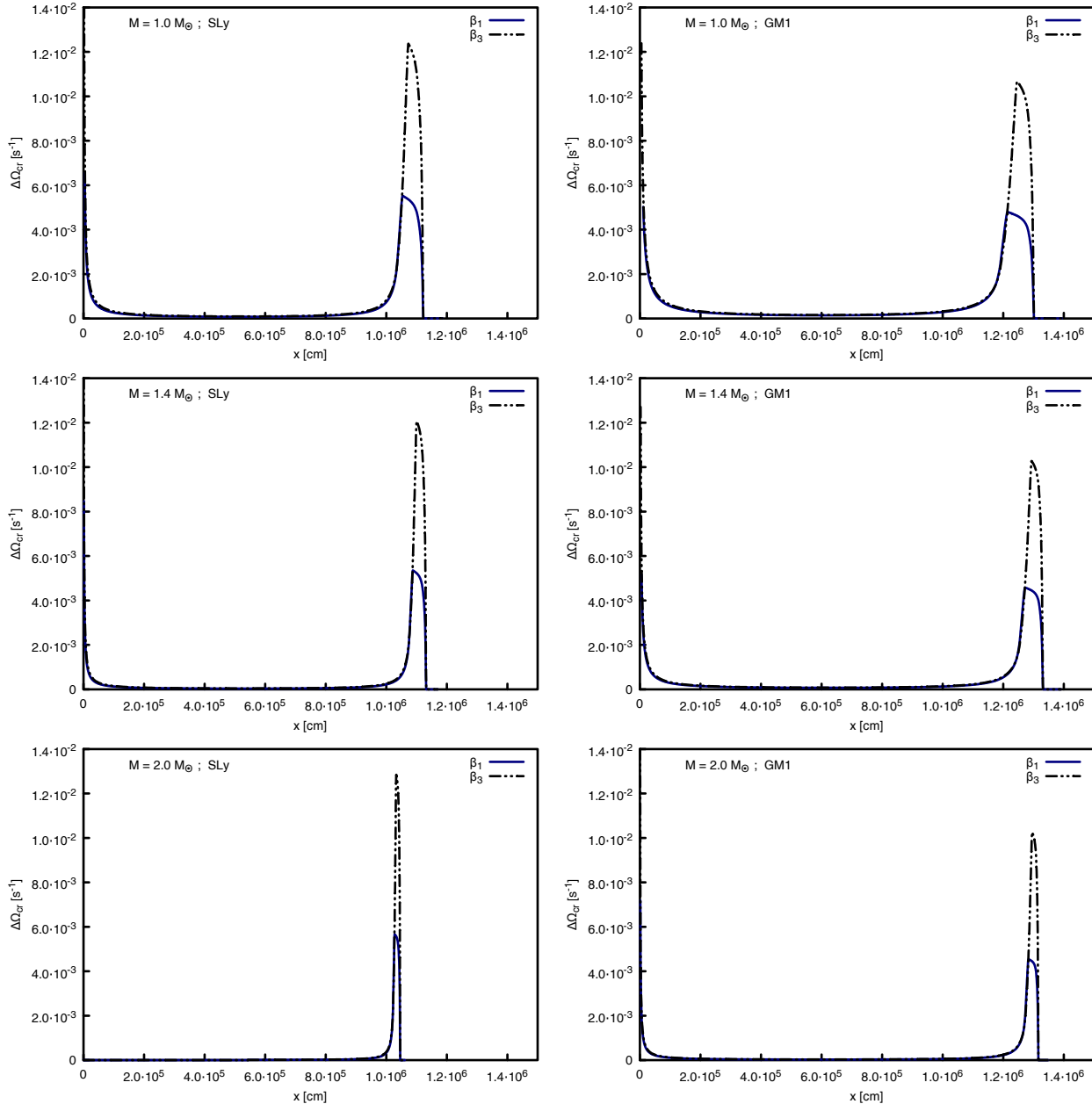


Figure 8. Plot of the critical lag $\Delta\Omega_{\text{cr}}(x)$ for different stellar models, with varying mass and equations of state. The pinning profiles used are plotted in figure 4 and we consider both the case $\beta = 1$ and the case $\beta = 3$. Note that in both cases ($\beta = 1$ and $\beta = 3$) the maximum amplitude of the pinning force is the same, so the difference in the maximum lag for the two cases is now entirely due to the different position in density of the maximum in the pinning force profile.

In the pre-glitch steady-state condition, due to the long timescales involved, we can assume $Y_\infty = 1$; but during a glitch this quantity cannot be calculated with the snowplow model as it depends on the detailed short-time dynamics of the vortices, and must thus be determined with hydrodynamical simulations such as those in Haskell, Pizzochero & Sidery (2012). As this is beyond the scope of the current paper, the quantity Y_{gl} is taken as a parameter of this model, and must be inferred from the observational data as shown in the next section.

The value Y_{gl} is needed for the evaluation of $\Delta\Omega_{\text{gl}}$, the jump in angular velocity of the normal component of the star

due to a glitch. This corresponds to the ratio between the angular momentum transfer ΔL_{gl} and the effective moment of inertia I_{eff} of the coupled fraction of matter during the glitch. One thus has that $I_{\text{eff}} = (1 - Q)I_{\text{tot}} + QY_{\text{gl}}I_{\text{tot}}$ and the requested quantity is therefore:

$$\Delta\Omega_{\text{gl}} = \frac{\Delta L_{\text{gl}}}{I_{\text{tot}} [1 - Q(1 - Y_{\text{gl}})]}. \quad (16)$$

A further parameter of the glitch that can be calculated is the relative acceleration of the crust. As illustrated in Pizzochero (2011) the desired relation follows from variation

at the glitch of the Euler equation for the normal component and angular momentum conservation:

$$\frac{\Delta\dot{\Omega}_{gl}}{\dot{\Omega}_{\infty}} = \frac{Q(1 - Y_{gl})}{1 - Q(1 - Y_{gl})}. \quad (17)$$

5 RESULTS AND OBSERVATIONS

In this section we test the model proposed here against observations. As the model has been developed for giant glitches we shall compare our results to observations of giant glitches in the Vela pulsar. The Vela (PSR B0833-45 or PSR J0835-4510) has a spin frequency $\nu \approx 11.19$ Hz and spin-down rate $\dot{\nu} \approx -1.55 \times 10^{-11}$ Hz s $^{-1}$; from relation 13 this value correspond to a maximum critical lag of $\Delta\Omega_{cr\max} = 8.6 \times 10^{-3}$ rad s $^{-1}$, where we have considered that the average time between glitches for this pulsar is 2.8 years. The glitch is usually described in terms of permanent steps in the frequency and frequency derivative and a series of transient terms that decay exponentially. It is well known that at least three transient terms are required, with decay timescales that range from months to hours (Flanagan 1996). Recent observations of the 2000 and 2004 glitch have shown that an additional term is required on short timescales, with a decay time of approximately a minute. Given that the detection in 2004 was only barely above the noise we shall refer to the January 2000 glitch. In this case the jump in angular velocity was of $\Delta\Omega_{gl} = 2.2 \times 10^{-4}$ rad s $^{-1}$ (Dodson, McCulloch & Lewis 2002; Dodson et al. 2007). This is a fairly typical value for giant glitches in the Vela, and we take it as our reference value. The relative step in frequency derivative corresponding to the transient term with the shortest decay timescale (1 minute) for this glitch is $\Delta\dot{\Omega}_{gl}/\dot{\Omega}_{\infty} \approx 18 \pm 6$ (1 σ error), and we assume that this is a good approximation to the *instantaneous* step in frequency derivative at the time of the glitch.

As explained in the previous section, the model has two free parameters that are the maximum value of the pinning force value f_{PM} and Y_{gl} : this means that, once a star has been fixed (by choosing the EoS, the mass M , and the superfluid fraction relation) we can use two observational quantities to constrain the parameters of the model and compare further observables to the quantities predicted by calculations. In particular, for each fixed star, we rescale the maximum of the pinning force in order to produce the maximum critical lag $\Delta\Omega_{cr\max}$ required to reproduce the average waiting time between glitches in the Vela. This allows us to calculate directly and univocally the angular momentum ΔL_{gl} from equation 15. As we want to reproduce a glitch of amplitude $\Delta\Omega_{gl} = 2.2 \times 10^{-4}$ rad s $^{-1}$, relation 16 can be rewritten in the following form

$$Y_{gl} = \frac{1}{Q} \left[\frac{\Delta L_{gl}}{I_{tot}\Delta\Omega_{gl}} + Q - 1 \right], \quad (18)$$

and therefore can be used to fix the coupled fraction of matter during the glitch. Tables 3, 4 and 5 give the fitting parameters for all the configurations tested. We can see that the value of the maximum pinning force f_{PM} does not change significantly with the total mass of the star. In these tables negative values of Y_{gl} are not given as they would not

be physically acceptable: a negative value would mean that there is not enough angular momentum to produce the required jump in angular velocity, even if we consider the core vorticity completely decoupled from the normal component of the star at the time of the glitch.

The remaining tables, numbered 6, 7 and 8, show the physical quantities that the “snowplow” model permits to evaluate. These are of course the angular momentum ΔL_{gl} transferred to the crust during the glitch and the relative step in frequency derivative. We can see that the order of magnitude for ΔL_{gl} is 10^{40} ergs, that is compatible with the upper limits on the glitch energy obtained from observations of the power wind nebula surrounding Vela (Helfand et al. 2001) and with the results found in Pizzochero (2011), where the same model is applied analytically with a polytropic EoS in Newtonian gravity. From these tables one can see that, for a particular choice of EoS and proton fraction, the angular momentum ΔL_{gl} stored by vortices decreases with the total mass of the star. This behaviour can be easily explained, as shown by Pizzochero (2011), in terms of the quantity x_{\max}/R_{ic} shown in the tables: ΔL_{gl} is obviously related to the number N_v of vortices stored at the peak (in tables 6, 7 and 8; see also eq. 15) – that however doesn’t change significantly with the mass – but it depends strongly on the ratio x_{\max}/R_{ic} which increases at higher masses. In Pizzochero (2011) (fig. 4) it is clearly shown that the angular momentum stored by the vortices at the peak decreases rapidly moving the position of the peak towards the outer crust. The quantity ΔL_{gl} also depends on the equation of state used (a stiffer EoS produces higher values of ΔL_{gl}) and on the pinning profile: the $\beta = 3$ condition, when other variables are fixed, gives lower values for the angular momentum, accordingly to the fact that the relative position of the peak with respect to the inner crust radius is higher.

The “snowplow” model permits to calculate also the step in spin-down rate immediately after a glitch, and this quantity is given in our tables as $\Delta\dot{\Omega}_{gl}/\dot{\Omega}_{\infty}$. It has been calculated only for acceptable values of Y_{gl} , and must be compared with the reference value of $\Delta\dot{\Omega}_{gl}/\dot{\Omega}_{\infty} = 18 \pm 6$, taken from the Vela 2000 glitch (Dodson, McCulloch & Lewis 2002). These values suggest that the $\beta = 3$ configurations are preferred and this can be considered in reasonable agreement with the microscopic results found by Gandolfi et al. (2008): they find that a realistic suppression factor for the pairing gap $\Delta(\rho)$ is $\beta \approx 1.5$ but, crucially, also that the maximum for $\Delta(\rho)$ is shifted at lower densities. This leads to a profile close to what we obtain for $\beta = 3$ in our model.

Finally let us remark that the results in tables 6, 7 and 8, for the (microscopically favoured) case $\beta = 3$, seem to indicate that a stiffer equation of state (GM1) is preferred as is a lower mass (possibly in the region of $1.4M_{\odot}$) for the Vela pulsar. Naturally such a quantitative conclusion is difficult to make on the basis of one observation and it would be highly desirable to have information on the short-timescale post-glitch behaviour not only of other Vela giant glitches, but also of other glitching pulsars. Note that short term components of the relaxation have not been measured for other giant glitchers, however the “snowplow” model can be used to predict waiting times, obtaining results which are consistent with observations (Haskell, Pizzochero & Sidery 2012).

Table 3. This table gives the fitting parameters f_{PM} (maximum of the pinning force per unit length) and Y_{gl} (fraction of coupled vorticity at the glitch) for all the considered configurations. x_{max} is the position (cylindrical radius) of the maximum critical lag. These values refer to a constant proton fraction $x_p(\rho) = 0.05$ (the corresponding fraction of moment of inertia due to the superfluid component of the star is $Q = 0.95$). Unphysical (negative) values for Y_{gl} are not reported (see text for details). Since the angular momentum transferred to the crust during a glitch is strongly dependant on the ratio $x_{\text{max}}/R_{\text{ic}}$ (see section 5), this quantity is also reported in table.

EoS	M (M_{\odot})	$\beta = 1$				$\beta = 3$			
		x_{max} (km)	$x_{\text{max}}/R_{\text{ic}}$	$f_{\text{PM}}/10^{15}$ (dyn cm $^{-1}$)	Y_{gl}	x_{max} (km)	$x_{\text{max}}/R_{\text{ic}}$	$f_{\text{PM}}/10^{15}$ (dyn cm $^{-1}$)	Y_{gl}
SLy	1.0	10.530	0.938	1.562	0.203	10.724	0.955	0.697	0.027
	1.1	10.654	0.945	1.581	0.148	10.829	0.960	0.704	0.009
	1.2	10.753	0.951	1.595	0.106	10.910	0.965	0.709	–
	1.3	10.827	0.956	1.606	0.074	10.968	0.968	0.713	–
	1.4	10.875	0.961	1.613	0.048	11.001	0.972	0.715	–
	1.5	10.897	0.965	1.616	0.027	11.010	0.975	0.716	–
	1.6	10.889	0.969	1.615	0.011	10.990	0.977	0.715	–
	1.7	10.847	0.972	1.609	–	10.937	0.980	0.711	–
	1.8	10.759	0.975	1.596	–	10.838	0.982	0.705	–
	1.9	10.600	0.979	1.572	–	10.667	0.985	0.694	–
2.0	10.279	0.982	1.525	–	10.332	0.987	0.672	–	
GM1	1.0	12.129	0.932	1.798	0.493	12.447	0.956	0.809	0.078
	1.1	12.315	0.939	1.825	0.389	12.604	0.961	0.819	0.051
	1.2	12.473	0.945	1.849	0.307	12.737	0.965	0.827	0.031
	1.3	12.604	0.950	1.868	0.242	12.844	0.968	0.834	0.015
	1.4	12.710	0.955	1.884	0.190	12.929	0.971	0.840	0.003
	1.5	12.792	0.959	1.896	0.148	12.992	0.974	0.844	–
	1.6	12.852	0.962	1.905	0.113	13.034	0.976	0.847	–
	1.7	12.890	0.966	1.910	0.083	13.055	0.978	0.848	–
	1.8	12.901	0.969	1.912	0.060	13.052	0.980	0.848	–
	1.9	12.885	0.972	1.910	0.040	13.022	0.982	0.846	–
	2.0	12.836	0.974	1.902	0.023	12.960	0.984	0.842	–
	2.1	12.744	0.977	1.889	0.007	12.854	0.985	0.835	–
	2.2	12.586	0.980	1.865	–	12.683	0.987	0.824	–
2.3	12.287	0.982	1.821	–	12.367	0.989	0.803	–	

6 CONCLUSIONS

In this paper we have extended the “snowplow” model for giant pulsar glitches of Pizzochero (2011) to incorporate relativistic background stellar models and realistic equations of state. In particular we test the model for the SLy and GM1 equations of state. Unfortunately these equations of state do not include information on beta equilibrium, so we use the proton fractions calculated by Zuo et al. (2004). It would of course be highly desirable to use proton fractions that are consistent with the individual equations of state in future work, in order to set stringent constraints. Furthermore we use, for the first time, the realistic profiles for the pinning forces per unit length calculated by Grill & Pizzochero (2012a) (see also Grill (2011); Grill & Pizzochero (2012b)), in order to evaluate the amount of angular momentum that can be transferred to the crust during a glitch.

The model contains three free parameters, the mass of the star M , the fraction of superfluid that is coupled to the crust during a glitch Y_{gl} , (which can only be estimated with dynamical simulations such as those of Haskell, Pizzochero & Sidery (2012)), and the maximum amplitude of the pinning force, f_{PM} . Note in fact that while the location of the maximum is precisely determined by the microphysical calculations of Grill & Pizzochero (2012a) (see also Grill (2011); Grill & Pizzochero (2012b)), the actual value of the

maximum can vary by factors of order unity or more as it depends on the poorly constrained value of the vortex tension. We thus treat it as a normalization and determine its value by requiring that the waiting time between glitches is of 2.8 years, as is approximately the case for Vela glitches. We then fit the size of the glitch to an average Vela glitch to obtain the value of Y_{gl} . In particular we take the value of the Vela 2000 glitch, $\Delta\Omega = 2.2 \times 10^{-4}$ rad s $^{-1}$ (Dodson, McCulloch & Lewis 2002).

Having determined the free parameters in our model, except for the mass of the NS which is free, we compare our results to the post glitch step in frequency derivative. Unfortunately the changes in $\dot{\nu}$ on short time scales after a glitch are observationally challenging to detect and it has been possible to fit for transient steps in frequency and frequency derivative on timescales of minutes after a glitch only for the Vela 2000 and 2004 glitch (Dodson, McCulloch & Lewis 2002; Dodson et al. 2007). Given that the detection is only barely above the noise for the 2004 glitch (Dodson et al. 2007) we fit to the values obtained for the 2000 glitch, which we assume to be a good approximation of the instantaneous post glitch behaviour. This justifies our choice of also fitting to the value of the jump in frequency of the Vela 2000 glitch.

The comparison of the model to the observational constraints first of all highlights that the general results of the analytic model of Pizzochero (2011) remain valid even in

Table 4. The fitting parameters given here (defined in table 3) refer to the proton fraction $x_p(\rho)$ proposed by Zuo et al. (2004), obtained with two-body forces.

EoS	M (M_\odot)	$\beta = 1$				$\beta = 3$			
		x_{\max} (km)	x_{\max}/R_{ic}	$f_{\text{PM}}/10^{15}$ (dyn cm $^{-1}$)	Y_{gl}	x_{\max} (km)	x_{\max}/R_{ic}	$f_{\text{PM}}/10^{15}$ (dyn cm $^{-1}$)	Y_{gl}
SLy	1.0	10.530	0.938	1.618	0.212	10.724	0.955	0.727	0.029
	1.1	10.654	0.945	1.637	0.152	10.829	0.960	0.735	0.007
	1.2	10.753	0.951	1.652	0.105	10.910	0.965	0.740	–
	1.3	10.827	0.956	1.663	0.067	10.968	0.968	0.744	–
	1.4	10.875	0.961	1.671	0.036	11.001	0.972	0.746	–
	1.5	10.897	0.965	1.674	0.010	11.010	0.975	0.747	–
	1.6	10.889	0.969	1.673	–	10.990	0.977	0.745	–
	1.7	10.847	0.972	1.666	–	10.937	0.980	0.742	–
	1.8	10.759	0.975	1.653	–	10.837	0.982	0.735	–
	1.9	10.600	0.979	1.628	–	10.666	0.985	0.723	–
2.0	10.279	0.982	1.579	–	10.332	0.987	0.701	–	
GM1	1.0	12.129	0.932	1.861	0.522	12.446	0.956	0.843	0.099
	1.1	12.315	0.939	1.890	0.415	12.605	0.961	0.854	0.070
	1.2	12.473	0.945	1.914	0.330	12.736	0.965	0.863	0.048
	1.3	12.604	0.950	1.934	0.262	12.844	0.968	0.870	0.029
	1.4	12.710	0.955	1.951	0.207	12.929	0.971	0.876	0.014
	1.5	12.792	0.959	1.963	0.162	12.992	0.974	0.880	0.002
	1.6	12.852	0.962	1.972	0.124	13.034	0.976	0.883	–
	1.7	12.888	0.966	1.978	0.092	13.055	0.978	0.884	–
	1.8	12.900	0.969	1.980	0.064	13.052	0.980	0.884	–
	1.9	12.885	0.972	1.977	0.039	13.022	0.982	0.882	–
	2.0	12.836	0.974	1.970	0.018	12.960	0.984	0.878	–
	2.1	12.744	0.977	1.956	–	12.854	0.985	0.871	–
	2.2	12.586	0.980	1.931	–	12.683	0.987	0.859	–
2.3	12.286	0.982	1.885	–	12.367	0.989	0.838	–	

our more physically realistic approach and the results are in general consistent for both equations of state for a reasonable range of neutron star masses. The glitch model presented here thus appears robust and compatible with the observations of giant glitches in the Vela and is, as shown in Haskell, Pizzochero & Sidery (2012), compatible with the average waiting time between giant glitches in other pulsars. This further reinforces the hypothesis that giant glitches are approximately periodic phenomena that occur close to the maximum lag that the pinning force can support in the crust, while smaller glitches may be triggered by random events such as crust quakes (Ruderman 1976; Ruderman, Zhu & Chen 1998) or vortex avalanches (Warszawski & Melatos 2008; Melatos & Warszawski 2009; Warszawski & Melatos 2011, 2012). Furthermore our results favour lower masses for the Vela pulsar (smaller than $1.5M_\odot$) and stiffer equations of state. Note however that such a quantitative conclusion is difficult to draw as not only are we comparing to a single observation but dynamical simulations have also shown that superfluid mutual friction will contribute significantly to the short term post-glitch spindown (Haskell, Pizzochero & Sidery 2012) as may friction at the crust/core interface (van Eysden & Melatos 2010). It will thus be necessary to further develop hydrodynamical glitch simulations to truly constrain the equation of state and the stellar mass.

Finally let us remark that in this paper we have assumed straight vortices that cross the core of the neutron star and are only weakly pinned at their extremities. Although the assumption of vortices that pass through the

star appears to be justified by microphysical estimates, that do not predict an interface of normal matter between the crust and core superfluid (Zhou et al. 2004), it may be the case that if the protons in the core are in a type II superconducting state this could lead to strong pinning also in the stellar interior (Ruderman, Zhu & Chen 1998; Link 2003). In this case not only would vortex motion be impeded, but it is also likely that turbulence will develop (Link 2011b,a). Note, however, that a large portion of the star may be in a type I superconducting state (Jones 2006) in which the magnetic field is not organised in flux tubes, but rather in macroscopic regions of normal matter, and the interactions may be much weaker (Sedrakian 2005) (although see Jones (2006) for a discussion of pinning in type I superconductors). Furthermore Babaev (2009) has recently shown that in the presence of strong entrainment or superfluid Σ^- hyperons, the interaction between vortices and flux tubes may be much weaker than generally assumed in the presence of type II superconductivity. In this paper we thus take the view that pinning in the core will be weak, although strong pinning of vortices to flux tubes is an intriguing possibility and will be the focus of a future publication (Haskell, Pizzochero & Seveso, in preparation).

Turbulence, on the other hand, is well known from laboratory superfluids and may play an important role in pulsar glitches (Peralta et al. 2006; Melatos & Peralta 2007; Peralta & Melatos 2009) and could couple the superfluid and the normal component on inter-glitch timescales in the presence of core pinning (Andersson, Sidery & Comer 2007). The in-

Table 5. This table is analogous to tables 3 and 4: here the proton fraction used is that calculated by Zuo et al. (2004) with three-body forces.

EoS	M (M_{\odot})	$\beta = 1$				$\beta = 3$			
		x_{\max} (km)	x_{\max}/R_{ic}	$f_{\text{PM}}/10^{15}$ (dyn cm $^{-1}$)	Y_{gl}	x_{\max} (km)	x_{\max}/R_{ic}	$f_{\text{PM}}/10^{15}$ (dyn cm $^{-1}$)	Y_{gl}
SLy	1.0	10.530	0.938	1.619	0.197	10.724	0.955	0.728	0.011
	1.1	10.654	0.945	1.638	0.133	10.829	0.960	0.735	–
	1.2	10.753	0.951	1.653	0.080	10.910	0.965	0.740	–
	1.3	10.827	0.956	1.664	0.036	10.968	0.968	0.744	–
	1.4	10.875	0.961	1.672	–	11.001	0.972	0.746	–
	1.5	10.897	0.965	1.675	–	11.010	0.975	0.747	–
	1.6	10.889	0.969	1.674	–	10.990	0.977	0.746	–
	1.7	10.847	0.972	1.667	–	10.937	0.980	0.742	–
	1.8	10.759	0.975	1.654	–	10.837	0.982	0.735	–
	1.9	10.600	0.979	1.629	–	10.666	0.985	0.724	–
2.0	10.279	0.982	1.580	–	10.332	0.987	0.701	–	
GM1	1.0	12.129	0.932	1.862	0.521	12.446	0.956	0.843	0.095
	1.1	12.315	0.939	1.891	0.413	12.605	0.961	0.854	0.065
	1.2	12.473	0.945	1.915	0.326	12.736	0.965	0.863	0.042
	1.3	12.604	0.950	1.935	0.257	12.844	0.968	0.870	0.022
	1.4	12.710	0.955	1.952	0.200	12.929	0.971	0.876	0.006
	1.5	12.792	0.959	1.964	0.153	12.992	0.974	0.880	–
	1.6	12.852	0.962	1.973	0.112	13.034	0.976	0.883	–
	1.7	12.888	0.966	1.979	0.077	13.055	0.978	0.885	–
	1.8	12.900	0.969	1.981	0.046	13.052	0.980	0.884	–
	1.9	12.885	0.972	1.978	0.017	13.022	0.982	0.882	–
	2.0	12.836	0.974	1.971	–	12.960	0.984	0.878	–
	2.1	12.744	0.977	1.957	–	12.854	0.985	0.871	–
	2.2	12.586	0.980	1.932	–	12.683	0.987	0.859	–
2.3	12.286	0.982	1.886	–	12.367	0.989	0.838	–	

clusion of turbulence in a hydrodynamical glitch simulations is, however, a complex matter as not only is the nature of the turbulence not known (see e.g. Andersson, Sidery & Comer (2007); Link (2011b,a)) but also the definition of pinning force per unit length must be revisited in the presence of a turbulent tangle. Such a fundamental issue should clearly be the focus of future work.

ACKNOWLEDGMENTS

This work was supported by CompStar, a Research Networking Programme of the European Science Foundation. BH acknowledges support from the European Union via a Marie-Curie IEF fellowship and from the European Science Foundation (ESF) for the activity entitled “The New Physics of Compact Stars” (COMPSTAR) under exchange grant 2449.

REFERENCES

- Adams P.W., Cieplak M., Glaberson W.I., 1984., Phys Rev B, 32, 171
- Alpar M.A., 1977, Ap.J. 213, 527
- Alpar M.A., Anderson P.W., Pines D., Shaham J., 1984, Ap.J. 278, 791
- Alpar M.A., Langer S.A., Sauls J.A., 1984, Ap.J. 282, 533
- Anderson P.W., Itoh N., 1975, Nature 256, 25
- Anderson P.W., Alpar M.A., Pines D., Shaham J., 1982, Philos.Mag. A 45, 227
- Andersson N., Sidery T., Comer G.L., 2006, MNRAS 368, 162
- Andersson N., Sidery T., Comer G.L., 2007, MNRAS 381, 747
- Babaev E., 2009, Phys.Rev.Lett 103, 231101
- Baym G., Pethick C., Pines D., 1969, Nature 224, 872
- Crawford F., Demianski M., 2003, ApJ 595, 1052
- Demorest P.B., Pennucci T., Ransom S.M., Roberts M.S.E., Hessels J.W.T., 2010, Nature 467, 1081
- Dodson R.G., McCulloch P.M., Lewis D.R., 2002, ApJL 564, L85
- Dodson R.G., Lewis D.R., McCulloch P.M., 2007, Ap&SS, 308, 585
- Donati, P., Pizzochero P.M., 2003, Phys.Rev.Lett. 90, 21
- Donati, P., Pizzochero P.M., 2004, Nu.Phys.A, 742, 363
- Donati, P., Pizzochero P.M., 2006, Phys.Lett.B, 640
- Douchin F., Haensel P., 2001, A&A 380, 151
- Epstein R.I., Baym G., 1988, Ap.J. 328, 680
- van Eysden C.A., Melatos A., 2010, MNRAS 409, 1253
- Espinoza C.M., Lyne A.G., Stappers B.W., Kramer M., 2011, MNRAS 414, 1679
- Flanagan C.S., 1996, “Pulsars: Problems & Progress”, ASP Conference Series, Vol. 105, Eds. S.Johnston, M.A. Walker & M.Bailes
- Gandolfi S., Illarionov A.Yu, Fantoni S., Pederiva F., Schmidt K.E., 2008., Phys Rev Lett., 101, 132501
- Glampedakis K., Andersson N., 2009., Phys Rev Lett., 102,

Table 6. This table shows, for the considered configurations, the physical quantities that the “snowplow” model permits to evaluate: the number N_v of vortices stored at the peak in critical lag just before the glitch, the angular momentum transferred to the crust ΔL_{gl} , and the step in frequency derivative on short timescales $\Delta\dot{\Omega}_{gl}/\dot{\Omega}_\infty$. Like table 3 (that gives the fitting parameters used), this one refers to a constant proton fraction that gives $Q = 0.95$.

EoS	M (M_\odot)	R (km)	$\beta = 1$			$\beta = 3$		
			N_v (10^{13})	ΔL_{gl} (10^{40} erg s)	$\Delta\dot{\Omega}_{gl}/\dot{\Omega}_\infty$	N_v (10^{13})	ΔL_{gl} (10^{40} erg s)	$\Delta\dot{\Omega}_{gl}/\dot{\Omega}_\infty$
SLy	1.0	11.855	3.041	3.889	3.124	3.154	1.216	12.184
	1.1	11.830	3.113	3.425	4.242	3.216	1.059	15.950
	1.2	11.797	3.171	2.996	5.622	3.265	0.919	–
	1.3	11.758	3.215	2.601	7.331	3.299	0.792	–
	1.4	11.705	3.244	2.235	9.476	3.319	0.677	–
	1.5	11.635	3.257	1.903	12.166	3.325	0.570	–
	1.6	11.545	3.252	1.595	15.629	3.313	0.477	–
	1.7	11.422	3.227	1.304	–	3.280	0.387	–
	1.8	11.260	3.175	1.033	–	3.221	0.304	–
	1.9	11.025	3.082	0.771	–	3.121	0.226	–
2.0	10.620	2.898	0.498	–	2.928	0.147	–	
GM1	1.0	13.940	4.034	11.480	0.931	4.249	2.741	7.086
	1.1	13.943	4.159	10.433	1.384	4.357	2.456	9.128
	1.2	13.940	4.267	9.429	1.927	4.449	2.180	11.657
	1.3	13.930	4.357	8.481	2.570	4.524	1.958	14.462
	1.4	13.913	4.430	7.599	3.330	4.584	1.743	17.882
	1.5	13.885	4.488	6.764	4.242	4.629	1.542	–
	1.6	13.845	4.530	5.977	5.344	4.660	1.355	–
	1.7	13.788	4.557	5.198	6.744	4.674	1.184	–
	1.8	13.715	4.565	4.543	8.336	4.672	1.020	–
	1.9	13.620	4.553	3.895	10.385	4.651	0.869	–
	2.0	13.495	4.519	3.284	12.999	4.606	0.727	–
	2.1	13.330	4.455	2.688	16.541	4.532	0.593	–
	2.2	13.095	4.345	2.104	–	4.411	0.460	–
2.3	12.713	4.140	1.481	–	4.195	0.327	–	

141101

Glampedakis K., Andersson N., 2011a, ApJ 740, L35
 Glendenning, N.K., Moszkowski, S.A. 1991, Phys. Rev. Lett. 67, 2414
 Grill F., 2011, PhD Thesis, University of Milan.
 Grill F., Pizzochero P.M., 2012a, Journal of Physics: Conference Series 342, 012004
 Grill F., Pizzochero P.M., 2012b, in preparation
 Haskell B., Pizzochero P.M., Sidery T., 2012, MNRAS 420, 658
 Helfand D. J., Gotthelf E. V., & Halper, J. P. 2001, ApJ, 556, 380
 Jones P.B., 2006, MNRAS 371, 1327
 Larson M.B., Link B., 2002, MNRAS, 333, 613
 Link B., 2003, Phys.Rev.Lett. 91 ,10110
 Link B., 2009, Phys.Rev.Lett. 102, 131101
 Link B., 2011a, preprint: arXiv:1105.4654
 Link B., 2011b, preprint: arXiv:1111.0696
 Melatos A., Peralta C., 2007, ApJ. 662, L99
 Melatos A., Warszawski L., 2009, ApJ. 700, 1524
 Middleditch J., Marshall F.E., Wang Q.D., Gotthelf E.V., Zhang W., 2006, ApJ, 625, 1531
 Page D., Prakash M., Lattimer J.M., Steiner A.W., 2011, Phys.Rev.Lett. 106, 081101
 Peralta C., Melatos A., Giacobello M., Ooi A., 2006, ApJ. 651,
 Peralta C., Melatos A., 2009, ApJ. 701, L75 1079
 Pines D., Shaham J., Alpar M.A., Anderson P.W., 1980,

Prog.Theor.Phys., Suppl. 69, 376

Pizzochero P.M., 2011, ApJ. 743, L20
 Ruderman M.A., Sutherland P.G., 1974, Ap.J. 190, 137
 Ruderman M., 1976, Ap.J. 203, 213
 Ruderman M., Zhu T., Chen K., 1998, Ap.J. 492, 267
 Sedrakian A., 2005, Phys.Rev.D 71, 3003
 Shternin P.S., Yakovlev D.G., Heinke C.O., Ho W.C.G., Patnaude D.J., 2011, MNRAS 41, L108
 Warszawski L., Melatos A., 2008, MNRAS 390, 175
 Warszawski L., Melatos A., 2011, MNRAS 415, 1611
 Warszawski L., Melatos A., 2012, preprint: arXiv:1203.4466
 Zhou X.-R., Schulze H.-J., Zhao E.-G., Pan F., Draayer J. P., 2004, Phys. Rev. C, 70, 048802
 Zuo W., Li Z.H., Lu G.C., Li J.Q., Scheid W., Lombardo U., Schulze H.-J., Shen C.W., 2004, Phys.Lett.B 595, 44

This paper has been typeset from a \TeX / \LaTeX file prepared by the author.

Table 7. The quantities ΔL_{gl} and $\Delta \dot{\Omega}_{\text{gl}}/\dot{\Omega}_{\infty}$ here reported follows from calculation base on the proton fraction proposed by Zuo et al. (2004) with two-body interactions. The corresponding fitting parameters are shown in table 4. $Q = I_s/I_{\text{tot}}$ is the global superfluid fraction of moment of inertia.

EoS	M (M_{\odot})	R (km)	Q	$\beta = 1$			$\beta = 3$		
				N_{v} (10^{13})	ΔL_{gl} (10^{40} erg s)	$\Delta \dot{\Omega}_{\text{gl}}/\dot{\Omega}_{\infty}$	N_{v} (10^{13})	ΔL_{gl} (10^{40} erg s)	$\Delta \dot{\Omega}_{\text{gl}}/\dot{\Omega}_{\infty}$
SLy	1.0	11.855	0.948	3.041	4.048	2.962	3.154	1.272	11.609
	1.1	11.830	0.945	3.113	3.565	4.036	3.216	1.108	15.210
	1.2	11.797	0.942	3.171	3.119	5.362	3.265	0.961	–
	1.3	11.758	0.938	3.215	2.708	7.005	3.299	0.828	–
	1.4	11.705	0.934	3.244	2.327	9.065	3.319	0.708	–
	1.5	11.635	0.930	3.257	1.981	11.650	3.325	0.596	–
	1.6	11.545	0.925	3.252	1.660	–	3.313	0.499	–
	1.7	11.422	0.920	3.227	1.357	–	3.280	0.405	–
	1.8	11.260	0.913	3.175	1.076	–	3.221	0.321	–
	1.9	11.025	0.905	3.082	0.803	–	3.120	0.239	–
2.0	10.620	0.890	2.898	0.518	–	2.928	0.153	–	
GM1	1.0	13.940	0.966	4.034	11.939	0.856	4.248	2.874	6.713
	1.1	13.943	0.964	4.159	10.850	1.292	4.357	2.559	8.719
	1.2	13.940	0.962	4.267	9.805	1.814	4.448	2.303	10.982
	1.3	13.930	0.961	4.357	8.820	2.433	4.524	2.047	13.792
	1.4	13.913	0.959	4.430	7.903	3.164	4.584	1.822	17.063
	1.5	13.885	0.956	4.488	7.034	4.041	4.629	1.612	20.994
	1.6	13.845	0.954	4.530	6.216	5.101	4.660	1.416	–
	1.7	13.788	0.952	4.556	5.463	6.367	4.674	1.237	–
	1.8	13.715	0.949	4.564	4.743	7.943	4.672	1.066	–
	1.9	13.620	0.946	4.553	4.051	9.948	4.651	0.909	–
	2.0	13.495	0.942	4.519	3.415	12.463	4.606	0.760	–
	2.1	13.330	0.938	4.455	2.796	–	4.532	0.620	–
	2.2	13.095	0.933	4.345	2.188	–	4.411	0.481	–
2.3	12.713	0.925	4.140	1.552	–	4.195	0.342	–	

Table 8. The proton fraction used for this table is the three-body forces model of Zuo et al. (2004). The corresponding fitting parameters are shown in table 5.

EoS	M (M_\odot)	R (km)	Q	$\beta = 1$			$\beta = 3$		
				N_v (10^{13})	ΔL_{gl} (10^{40} erg s)	$\Delta \dot{\Omega}_{\text{gl}}/\dot{\Omega}_\infty$	N_v (10^{13})	ΔL_{gl} (10^{40} erg s)	$\Delta \dot{\Omega}_{\text{gl}}/\dot{\Omega}_\infty$
SLy	1.0	11.855	0.931	3.041	4.049	2.960	3.154	1.272	11.607
	1.1	11.830	0.924	3.113	3.567	4.034	3.216	1.108	–
	1.2	11.797	0.916	3.171	3.120	5.360	3.265	0.961	–
	1.3	11.758	0.908	3.215	2.708	7.002	3.299	0.828	–
	1.4	11.705	0.899	3.244	2.328	–	3.319	0.708	–
	1.5	11.635	0.888	3.257	1.981	–	3.325	0.597	–
	1.6	11.545	0.876	3.252	1.661	–	3.313	0.499	–
	1.7	11.422	0.862	3.227	1.358	–	3.280	0.405	–
	1.8	11.260	0.844	3.175	1.076	–	3.221	0.321	–
	1.9	11.025	0.820	3.082	0.803	–	3.120	0.239	–
2.0	10.620	0.779	2.898	0.518	–	2.928	0.153	–	
GM1	1.0	13.940	0.962	4.034	11.944	0.856	4.248	2.874	6.712
	1.1	13.943	0.959	4.159	10.854	1.292	4.357	2.559	8.718
	1.2	13.940	0.957	4.267	9.809	1.813	4.448	2.303	10.981
	1.3	13.930	0.953	4.357	8.824	2.432	4.524	2.047	13.791
	1.4	13.913	0.950	4.430	7.906	3.163	4.584	1.822	17.061
	1.5	13.885	0.946	4.488	7.037	4.039	4.629	1.612	–
	1.6	13.845	0.942	4.530	6.218	5.099	4.660	1.416	–
	1.7	13.788	0.937	4.556	5.465	6.365	4.674	1.237	–
	1.8	13.715	0.931	4.564	4.744	7.939	4.672	1.066	–
	1.9	13.620	0.925	4.553	4.052	9.944	4.651	0.909	–
	2.0	13.495	0.917	4.519	3.416	–	4.606	0.760	–
	2.1	13.330	0.907	4.455	2.797	–	4.532	0.620	–
	2.2	13.095	0.894	4.345	2.188	–	4.411	0.481	–
2.3	12.713	0.873	4.140	1.553	–	4.195	0.342	–	